Influence of Recycled High-Density Polyethylene Fibers on the Mechanical and Electrochemical Properties of Reinforced Concrete

Alejandro Flores Nicolás [1,*], Elsa C. Menchaca Campos [1], Mario Flores Nicolás [2], José J. Martínez González [1], Omar A. González Noriega [1] and Jorge Uruchurtu Chavarín [1]

[1] Centro de Investigación en Ingeniería y Ciencias Aplicadas, Universidad Autónoma del Estado de Morelos, Av. Universidad 1001, Col. Chamilpa, Cuernavaca C.P. 62209, MOR, Mexico; elsa.menchacac@uaem.edu.mx (E.C.M.C.); jose.martinezgon@uaem.edu.mx (J.J.M.G.); ingomarglezn@gmail.com (O.A.G.N.); juch25@uaem.mx (J.U.C.)

[2] Instituto de Ingeniería, Universidad Nacional Autónoma de México, Circuito Escolar s/n, Ciudad Universitaria, Coyoacán C.P. 04510, CDMX, Mexico; mfloresn@iingen.unam.mx

* Correspondence: alejandro.floresnic@uaem.edu.mx

Abstract: The quantity of different plastics generated after consumption is an impact factor affecting the environment, and the lack of recycling generates solid waste. The purpose of this work is to incorporate high-density recycled polyethylene fibers (HDPE) for possible use as concrete reinforcement. Physical and mechanical properties from recycled fibers were analyzed, such as density, absorption, and stress resistance, as well as workability, air content, porosity, concrete compression, and flexural strength properties. Samples were prepared with a low fiber content of 0.2% and 0.4%, as a substitution for sand weight, and lengths of 10 and 30 mm. To study corrosion phenomena, the specimens were exposed to a saline environment containing 3% sodium chloride for 365 days, and the electrochemical techniques including half-cell potential (HCP), electrochemical noise (EN), linear polarization resistance (LPR), and electrochemical impedance spectroscopy (EIS) were applied. The results showed a 4.8% increase in compressive strength with a low fiber percentage and short geometries, while flexural strength increased marginally by 2.3% with small quantities of HDPE fibers. All these factors contribute to greater material durability, less permeability, and crack control. A positive effect of fibers with short dimensions on the corrosion processes of a steel bar was observed, with the fibers acting as a physical barrier against the diffusion of chloride ions.

Keywords: recycling; high-density polyethylene fibers; reinforced concrete; mechanical properties; electrochemical techniques; corrosion

1. Introduction

Corrosion of steel is the main problem in concrete structures, which is caused by exposure to different aggressive environments that affect its durability and useful life. Cement paste's basic pH passivates a rod and protects it from the external environment, but this protection can be reduced or even nullified by high porosity or the presence of cracks [1], in addition to different factors such as the design of the paste, the preparation of the mixture, aggregate quality, the curing process, and the chemical properties of concrete. Passivation breakdown in concrete reinforcing steel in metal is caused by the following two types of corrosion: localized attack promoted by the presence of chloride ions and carbonation [2,3]. Compared with the damage caused by carbonation degradation, chloride-induced corrosion is more harmful since it causes localized attack, which is a type of heterogeneous corrosion [4]. The corrosion phenomenon can be interpreted based on thermodynamic properties, such as the electrochemical potential, and kinetic properties, such as the amount of electrical charge transferred (i.e., current density) [5]. To reduce the nocive effects of

corrosion, numerous investigations have addressed the need to obtain alternative synthetic materials for conventional reinforced concrete. With global plastic production rapidly increasing, numerous plastics are incorporated into the environment during their life cycle, and, with a great volume of waste being generated daily without further treatment, this represents an even greater problem since these plastics are not degraded by their surroundings [6,7]. Many of them are discarded due to their high demand in the consumer market, the most popular being polyethylene (PE), polypropylene (PP), polyvinyl chloride (PVC), polyethylene terephthalate (PET), and polystyrene (PS) [6,8]. Polyethylene-based plastics remain in the environment for long periods due to a lack of functional groups for their microbial degradation [9]. High-density polyethylene (HDPE) is a thermoplastic semi-crystalline polymer, belonging to polyolefins, fabricated from ethylene polymerization with the help of catalysts [10]. It is mainly used as a basic thermoplastic employed as industrial packaging due to its good mechanical properties, ease of processability, and low cost [11]. These subtle characteristic differences are caused by technological polymerization variations, catalyzer residues, polymeric chain molecular structures, and the additives used [12]. Furthermore, it is one of the most widely used plastics on the market, found in milk bottles, detergents, cosmetics, etc., resulting in a great quantity of pollution waste after product consumption that is not easily recycled. Therefore, implementing a recycling process offers an opportunity to improve economic viability and environmental sustainability for plastic residue processing [13]. Nowadays, research into contaminant residues from post-consumption goods is an attractive alternative to address potential environmental problems by reducing or eliminating them and improving resource conservation [14]. This waste can be recycled and applied in the construction industry as alternatives in reinforced materials with synthetic fibers, representing material characteristic solutions with technical and economic viability [15]. Many researchers have tested synthetic fibers as reinforcing concrete materials and have determined the appropriate quantities for the development of crack resistance and the diminishment of crack width in concrete, thus developing crack resistance, ductility, and tenacity [16,17]. Variable results were shown in fresh concrete workability, and many authors have reported a reduction in the increased substitution level for plastic fibers [18–20]. Regarding the mechanical properties of concrete reinforced with HDPE fibers, Malagavelli and Patura [21] analyzed HDPE fibers from cement bag residues, specifically compression and stress resistance, using 0.5–6% fibers, the results showed an increase of 2% in concrete compression and flexural resistance using fibers up to 2% maximum. Pesic et. al. [22] incorporated simple extrusion tests of HDPE recycled fibers and reported the mechanical results obtained from a concrete traction resistance and rupture module, with a marginal increase between 3% and 14% in the presence of 0.75–1.25% of HDPE fibers improving cracking capacity properties. Hossain et al. [23] investigated the durability of reinforced concrete with the addition of HDPE fibers through accelerated corrosion and obtained results showing that the HDPE sample presented a lower percentage of cracks and less chipping; furthermore, the corrosion was higher compared with the other samples. Additional advantages can be mentioned, including a lower weight when compared with steel and the absence of corrosion in these fibers [24]. In addition, the soft superficial texture and absence of reactivity of HDPE results in weak unions of the concrete matrix, thus reducing the mechanical as well as the durability performance, along with an increase in HDPE [25]. Therefore, the main objective of this work was the experimental study of the behavior of recycled HDPE fibers, with different proportions and geometric dimensions, on the physical, mechanical, and electrochemical properties of reinforced concrete, such as porosity, compressive and flexural strength, and the corrosion rate resistance of steel.

2. Materials and Methods

2.1. Materials

In this work, Portland cement CPC 30 R was used according to the international ASTM C150 standard [26], using sand with a particle diameter of 4.75 mm, obtained from a

riverbed, and crushed gravel with a maximum diameter size of 19 mm, as specified by the ASTM C136 standard [27], tap water, and HDPE recycled synthetic fibers.

2.2. HDPE Recycled Fibers

High-density polyethylene is a thermoplastic material composed of carbon and hydrogen atoms connected in a predominantly linear way [28]. HDPE is one of the most used plastics found in milk bottles, detergents, cosmetics, and drums, and as post-consumer products, they produce a large amount of waste contaminants that are not easily recycled. Synthetic fibers were obtained from detergent bottles collected in landfills, rivers, and streams in the state of Guerrero, Mexico. Subsequently, the bottles were cleaned, eliminating grease and dust contaminants, and then they were cut manually excluding the top and bottom, using the middle of the bottle to obtain a uniform thickness. Two different lengths were cut as follows: 10 mm short and 30 mm long, 3 to 4 mm wide and 0.05 mm thick, as seen in Figure 1. The reason for these dimensions was to find the optimal fiber size and its relationship to mechanical properties [29].

Figure 1. HDPE long recycled fiber.

2.3. Physical and Mechanical Properties of the Fibers

Plastic fibers were obtained from material residues without knowing their physical properties; therefore, density and absorption were obtained. The water absorption percent was obtained using the differences in weight method, according to the ASTM D570 standard [30]. Five measurements for each 30 HDPE fiber samples were performed using a Denver Instrument 0.0001 g precision electronic balance. The fibers were immersed in distilled water for 24 h, and afterward, they were dried with a cloth and weighed at the saturation point. The calculations were obtained using the following Equation (1):

$$\%A = \frac{wh - ws}{ws} \times 100,$$ (1)

where *wh* is the fiber weight and *ws* is the fiber weight after saturation. The recycled fiber apparent density calculation was obtained as the relation of weight and volume determining the fiber density [31]. To obtain the density, the immersion method was used. Five samples, thirty fiber pieces each, were water-saturated for 24 h and weighed using a Denver Instrument 0.0001 g precision electronic balance. Samples were deposited in 50 mL probes, and distilled water was poured in a 30 mL gauge and calculated according to the ASTM D792 standard [32] using the following Equation (2) [33,34]:

$$\rho = \frac{m}{vd},$$ (2)

where *r* is the density, *m* the average fiber saturated mass, and *vd* is the volume displaced. A stress resistance test was performed using parameters according to the ASTM D638 standard [35], covering the plastic materials. The dimensions of the specimens are shown

in Figure 2a, using type I from the standard. A 2000 kN maximum load MTS model 3156 universal press, with a 0.2 mm/min load speed, was used as shown in Figure 2b.

(**a**)

(**b**)
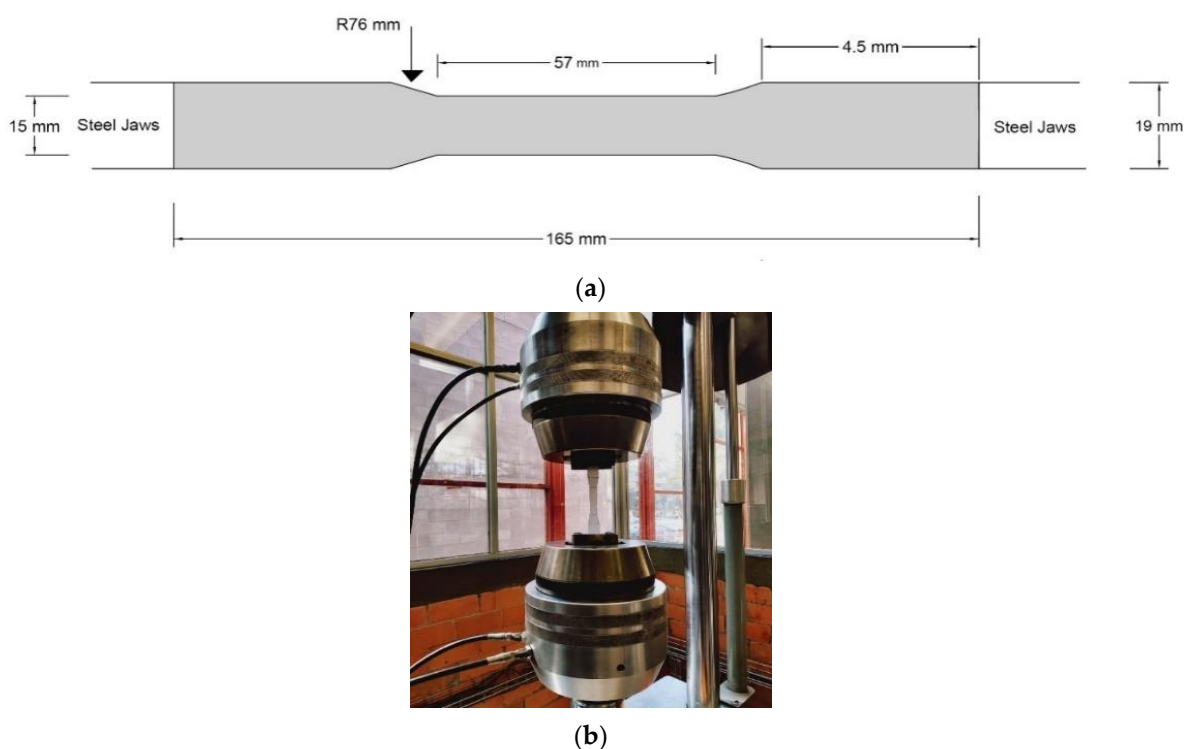
Figure 2. (**a**) Stress test sample dimensions for traction tests. (**b**) HDPE recycled fiber stress test.

2.4. Physical and Mechanical Tests of the HDPE Fibers

The HDPE fiber absorption and density results are shown in Table 1, indicating three polymeric compound diffusion mechanisms [36]. The first implies water molecule diffusion in the micro-spaces between polymeric chains; the second is capillary transport in interfacial voids between the fibers and polymeric matrix; and the third involves micro-cracks in the polymeric matrix [36]. The results show HDPE fibers with a low water absorption percentage of around 0.255%, due to the hydrophobic nature of the HDPE fibers, and some material micro-cracks, and the HDPE recycled fibers' density is 0.955 g/cm^3. These results are similar to those reported in the literature [22,33,37].

Table 1. HDPE recycled fibers' physical properties.

Fiber	Absorption (%)	Density (g/cm^3)	Reference
HDPE	---	0.926	[37]
HDPE	---	0.952	[33]
HDPE	---	0.952	[22]
HDPE	0.255	0.955	This study

In Figure 3, the HDPE recycled fibers' direct stress–strain curve is observed, and the data on the mechanical properties are shown in Table 2. The results highlight the material rupture maximum force, with an average value of 15 MPa, and lower stress resistance when compared with pure HDPE, with 25.7 and 28.8 MPa [38,39], and other recycled fibers presenting 37.7 MPa [22]. This could be due to several factors including use, wear, material degradation, and the recycling process.
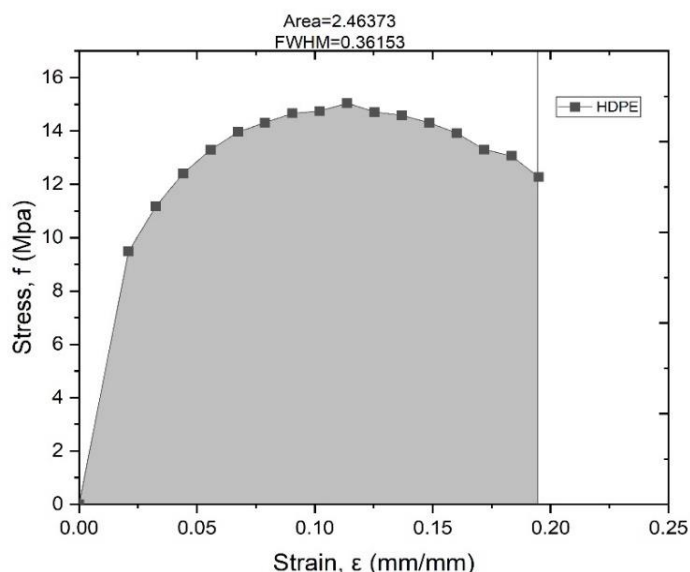
Figure 3. HDPE fiber stress–strain curve graph.

Table 2. HDPE recycled fibers' mechanical properties.

Properties	Units	HDPE
Tensile strength	MPa	15.05
Elasticity modulus	MPa	463
Toughness	N.mm	2.46

The elasticity module shows a value of 463 MPa, similar to other results reported in the literature [22,38], indicating that recycled HDPE fibers are a flexible material due to the high values of the elasticity module, due to the module's high values indicating a rigid material, and vice-versa. The stress value is used to describe a combination of resistance and ductility properties, evaluating the total area under the stress–strain curve [38]. A 2.46 MPa stress value was obtained, indicating less material energy impact absorption.

2.5. Concrete Mix Proportions

For concrete preparation, a sample control without fiber content was obtained, and samples with 0.2% and 0.4% HDPE recycled fibers added with respect to the fine aggregate (sand) weight were prepared. The w/c relation was 0.54, and Table 3 shows the detailed mixed proportions utilized.

Table 3. Concrete dosage 1 m^3.

Material	kg/m^3	Fiber 0.2%	Fiber 0.4%
Cement	366.07	366.07	366.07
Water w/c = 0.54	197.65	197.65	197.65
Gravel	1047.65	1047.65	1047.65
Sand	650.63	649.33	648.03
HDPE fiber	0	1.30	2.60

The procedure for the preparation of the concrete mix was carried out using a Husky industrial mixer with a 6.5 hp motor and a speed of 27–31 rpm. The materials were poured in the following order: first, coarse aggregate, then water, fine aggregate, cement, and finally, the HDPE fibers were incorporated into the paste, being distributed randomly. After pouring all the materials, a time of 4 min was given to mix all the aggregates, and then it was left to stand for 2 min, during which time a rod was used to stir part of the concrete

in the reduced areas of the pot to avoid lumps in the paste. Finally, it was stirred for 3 more minutes to pour it into the corresponding molds. The paste's physical characteristics were determined using the ASTM C 143 [40] standard for slump and the ASTM C 231 [41] standard for water content measurement. The nomenclature used for mechanical testing is presented in Table 4.

Table 4. Sample nomenclature.

Material	Percent Fibers (%)	Dimension (mm)	Nomenclature
Cement	-	-	CO
	0.2	30	LH-02
	0.2	10	CH-02
	0.4	30	LH-04
	0.4	10	CH-04

2.6. Specimen Preparation

Twelve cylinders were prepared for each design with dimensions of 150 mm diameter and 300 mm height, according to ASTM C31 [42]. The mechanical compression tests are shown in Figure 4. The tests were performed for 7 and 28 days after curing the specimens in water, covering the specimens' tops and bottoms with neoprene plates. A 120-ton universal machine was used with a loading rate between 0.15 and 0.35 MPa/s, as indicated in the ATM C 39 standard [43].


(**a**) (**b**)
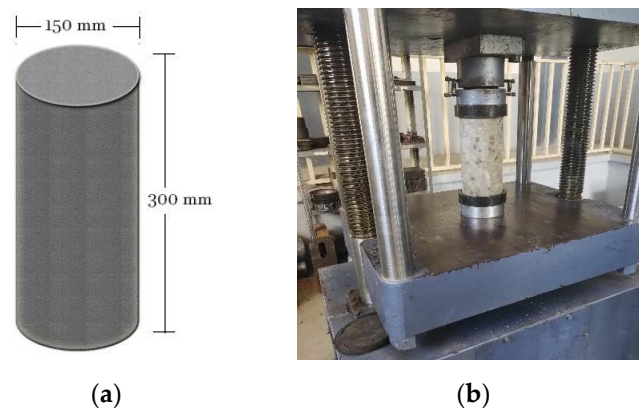
Figure 4. Mechanical tests (**a**) Sample dimensions. (**b**) compressive strength.

A flexural strength or rupture module (Rm) concrete resistance test was performed. First, 6 standard rectangular bars per sample were fabricated with dimensions as follows: 500 mm long, 150 mm wide, and 150 mm high. Then, testing after 28 curing days was performed, using the specimen's loading using the third point method. A constant speed of 0.86 and 1.21 MPa/min was applied until fracture occurred, according to the ASTM C78 standard [44]. The Rm is calculated according to Equation (3).

$$Rm = \frac{Pl}{bd^2},$$

(3)

where Rm is the rupture module, P is the applied loading, l is the distance between supporting points, b is the width, and d is the average slope sample. For the electrochemical techniques, cubic molds with the dimensions shown in Figure 5 were prepared as follows: 3 bars of low-carbon steel 1018 (diameter 3/8″), with a 35 mm overlap of the paste with the bottom rod; the exposed area of the steel was 2230 mm^2.
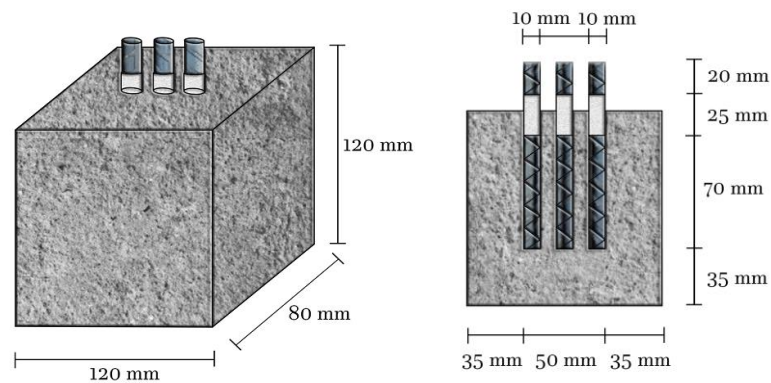
Figure 5. Dimension of the samples used for electrochemical techniques.

2.7. Electrochemical Techniques

2.7.1. Half-Cell Potential (HCP)

The half-cell potential (HCP) is a non-destructive method to measure the probability of corrosion on the metal surface and is interpreted with the parameters of the ASTM C-876-09 standard [45]. The operating principle of the HCP is that the electrical activity of the steel reinforcement and the concrete, considering the steel as an electrode and the concrete as an electrolyte, show a different electrochemical potential, resulting in detectable potential gradients at the surface of the concrete, which is measured and recorded as corrosion potential (Ecorr) [46,47]. The result is interpreted as the possibility of corrosion at a certain location of the concrete but cannot be used to firmly state the corrosion profile itself, such as the location, size, and shape of corrosion [48].

Corrosion potentials were monitored after 24 h of partial immersion in the salt solution and were configured with a silver/silver chloride-saturated reference electrode (Ag/AgCl) and working electrode w1, both connected with a voltmeter. Table 5 shows the risk criteria for interpreting the corrosion potential measurements of reinforcing bars embedded in concrete, with a saturated copper/copper sulfate (Cu/CuSO$_4$) electrode value conversion performed in the Ag/AgCl electrode values.

Table 5. Corrosion risk criteria for reinforced concrete.

Reference Electrode (mV)		Corrosion Probability
Cu/CuSO$_4$	Ag/AgCl	
>-200	>-150	Probability of corrosion 10%
-200 to -350	-150 to -300	Uncertain
<-350	<-300	Corrosion probability over 90%

2.7.2. Electrochemical Noise (EN)

The measurement of electrochemical noise (Rn) is a non-destructive method. The principle of the method, when applied to bare metal, is to achieve a measurement of the rate of equilibrium electrochemical reactions through the anodic reaction, for example, the dissolution of iron and the cathodic reaction associated with the reduction of oxygen [49]. Noise monitoring was carried out using potentiostat equipment from Gill AC-ACM Instruments. The electrochemical cell configuration was carried out with two electrodes, i.e., w1 and w2, one of them a nominally identical steel electrode as a counter electrode [50] and the second an Ag/AgCl reference electrode. A total of 1024 data points were collected at a rate of 1 point per second with an interval of 30 mV. The simplest parameters were obtained by simple combinations of the standard deviation (or other statistical parameters) of potential and current [51]. The ratio of the standard deviations of potential (σV) and cur-

rent intensity (σI) is called electrochemical noise resistance (R_n) as shown in the expression in Equation (4) [52].

$$R_n = \frac{\sigma V}{\sigma I},\tag{4}$$

Several researchers have analyzed the relationship between noise resistance (*Rn*) and polarization resistance (*Rp*), and some claim that the two are equivalent in some systems [51]. As *Rn* is equivalent to the biasing resistance (*Rp*), *Rp* can be replaced in Equation (5) by *Rn*, resulting in Equation (6) [53–55].

$$R_p = \frac{B}{i_{corr}},\tag{5}$$

$$i_{corr} = \frac{B}{R_n},\tag{6}$$

The type of corrosion occurring on the metal can be determined by a statistical parameter of the electrochemical noise, called the pitting index or localization, which is calculated by the ratio of the standard deviation in current (σI) and the root mean square current (I_{rms}). Table 6 shows the range of localization index values for the type of corrosion in metal [56].

$$L.I = \frac{\sigma I}{I_{rms}},\tag{7}$$

Table 6. Range of location index values.

Location Index	Type of Corrosion
0.001–0.01	Generalized
0.01–0.1	Mixed
0.1–1	Localized
>1	Start of pitting

2.7.3. Linear Polarization Resistance (LPR)

This electrochemical method is based on the measurement of the polarization resistance (LPR) of the metallic medium at the interface of a constant corrosion potential, where the corrosion rate expressed in terms of the dissolution current density of the metal is inversely proportional to the polarization resistance [57]. In the LPR technique, a small voltage signal was applied between -50 mV and $+50$ mV, according to ASTM G-59 [58], at a sweep rate of 60 mV/min. The slope of the resulting curve over the corrosion potential Ecorr is the polarization resistance, as shown in Equation (8) [59].

$$R_p = \frac{\Delta E}{\Delta I},\tag{8}$$

Equation (6) is used to calculate i_{corr} when the steel reinforcement is in the passivation stage, $B = 52$ mV, and when the armor is in the corrosion phase, $B = 26$ mV, where βa and βc are the Tafel constants in the anodic and cathodic processes, according to the following expression [60]:

$$B = \frac{\beta a \times \beta c}{2.303(\beta a + \beta c)},\tag{9}$$

During the monitoring of corrosion in reinforced concrete, a constant $B = 26$ mV was applied [61]. Using the values of current density (i_{corr}) and corrosion rate, the service life of the reinforcing steel in concrete can be estimated [62]. According to Flores-Nicolás et al. [63], for i_{corr} values lower than 0.1 $\mu A/cm^2$, the corrosion condition of the steel bar is negligible; for values in the range of 0.1 to 0.5 $\mu A/cm^2$, the level is moderate; for values from 0.5 to 1 $\mu A/cm^2$, the level is high; and finally, for values higher than 1 $\mu A/cm^2$, the corrosion degree is very high in the steel/concrete system.

2.7.4. Electrochemical Impedance Spectroscopy (EIS)

Electrochemical impedance spectroscopy (EIS) is a technique for characterizing a wide variety of electrochemical systems and can be used to investigate the dynamics of bound or moving loads in the volume of interface regions or any liquid or solid material. It assumes that a relatively elaborate circuit can represent the behavior of steel embedded inside the concrete [64]. EIS can be considered a quantifying method because it not only measures polarization resistance but also evaluates physical processes within the concrete and at the steel/concrete interface [65].

For the application of the EIS technique, the frequency range from 0.01 Hz to 10,000 Hz and an applied signal voltage of ±20 mV were set. ACM potentiostat equipment and the electrochemical cell consisting of 2 working electrodes, i.e., w1 and w2, one of them a nominally identical steel bar counter electrode and the second an Ag/AgCl reference electrode, were used.

3. Results

3.1. Freshly Mixed Concrete with Fibers

The workability of concrete paste is an indicator of the quality control of materials such as fine and coarse aggregates with the cementitious matrix. When adding synthetic fibers at more than 0.4%, the workability is reduced between 20% and 35%, maybe due to the fibers' flexibility resulting in less aggregate movement resistance [19]. As shown in Table 7, the air content increases in the LH-04 sample. This fact is probably due to the length of the fiber, which produces a greater quantity of voids at the time of compaction of the concrete with respect to the control concrete. On the other hand, the CH-02 sample has a lower quantity of air due to the presence of short fibers, showing better distribution within the cement matrix structure.

Table 7. HDPE concrete mixture properties.

Concrete	Slump (mm)	Air (%)
CO	140	2.1
CH-02	110	1.4
CH-04	90	1.5
LH-02	110	1.8
LH-04	100	2.3

3.2. Concrete Porosity

Concrete porosity is directly related to the quantity of voids present in the produced material. The percent porosity was calculated from the obtained air content results according to Equation (10) [66]:

$$p = \frac{\left(\frac{w}{c}\right) - 0.36h + \left(\frac{A}{c}\right)}{0.317 + 1\left[\left(\frac{1}{pf}\right)\left(\frac{Af}{c}\right)\right] + \left[\left(\frac{1}{pg}\right)\left(\frac{Ag}{c}\right)\right] + \left(\frac{A}{c}\right)}, \tag{10}$$

where w/c is the water–cement ratio, h is the cement hydration (0.7 for this work), A is the air volume trapped, pf and pg are the density of fine and coarse aggregates, and Af and Ag are the gravel and sand quantities. Figure 6 presents the porosity percent values of the concrete samples. The addition of synthetic fibers in the LH-04 sample resulted in an increase in porosity due to the fibers' form and dimension. Consequently, the samples present greater paste permeability when compared with the control sample; this fact can directly affect its compressive strength [67]. When short fibers were aggregated, a decreasing porosity was observed as a result of fiber geometry, beyond the concrete matrix pore quantity, altering its mechanical properties.
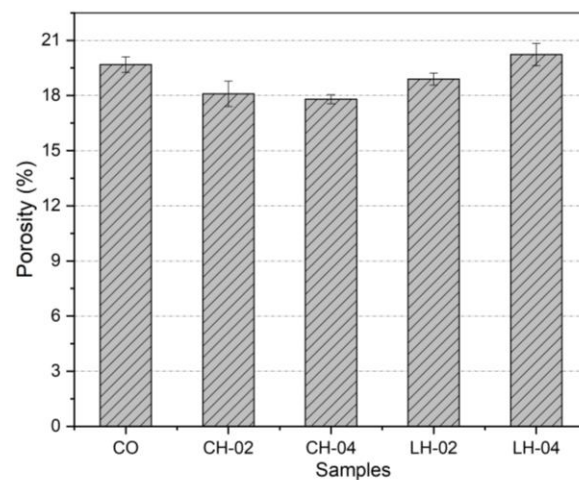
**Figure 6.** Concrete porosity with reinforcement fibers.

3.3. Compressive Strength

The concrete compressive strength (f'c) results from 7 and 28 curing days can be observed in Figure 7, where the CH-02 sample presents a 34 MPa f'c value, showing a 4.8% increase concerning the 32.5 MPa concrete control sample. This is due to a lower fiber surface area and better distribution of short fibers within the concrete matrix. Therefore, cracks appearing within the matrix have to take a winding path, resulting in a demand for more energy to propagate, which in turn increases the ultimate load [68]. Contrary to the long fiber aggregate quantity, as shown in sample LH-02, with an 8% f'c, an observed decrease in fibers added, comes from the fiber geometry in the cement matrix. Therefore, when increasing the amount of synthetic fibers in the LH-04 and CH-04 samples, having long and short lengths, the concrete f'c diminishes by 12%. This fact is due to the increase in synthetic fiber volume and greater fiber surface area, as well as weak structure cohesion and reinforcement and polymer particles acting as barriers avoiding cement adhesion [68].
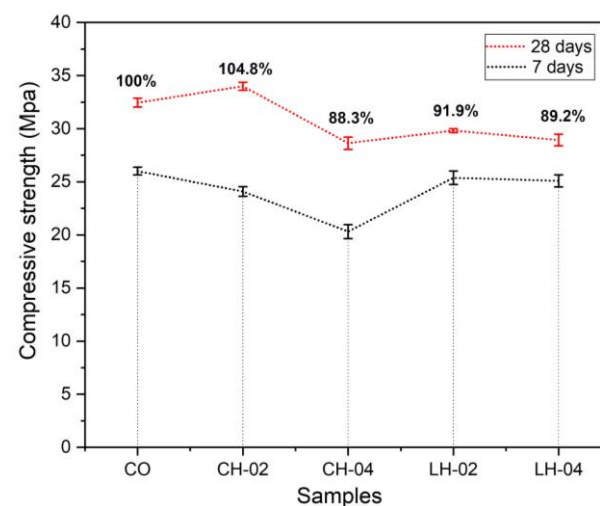
**Figure 7.** Compressive strength of concrete reinforced with HDPE fibers.

Failures of the concrete control sample generated during compression testing are presented in Figure 8a, showing a larger size crack on the cylinder top, which is responsible for the specimen sample rupture. Figure 8b presents the HDPE fiber sample, where the rupture was generated on both sides of the cylinder, forming several cracks all over and indicating that the sample presents higher ductility when compared with the control sample.

(**a**)   (**b**)
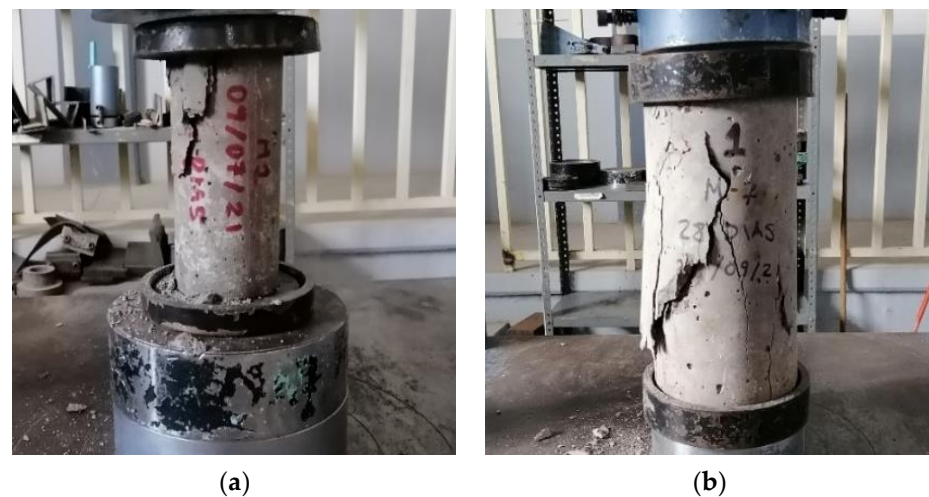
Figure 8. Compressive strength after 28 days of curing: (**a**) CO and (**b**) LH-04.

3.4. Flexural Strength

Figure 9 presents the flexural strength (f'f) results obtained for concrete reinforced with the addition of HDPE fibers. The LH-02 sample presents a slight increase in the f'f resistance of 2.3%, which could be due to the flexibility provided by the long fibers. When short-length fibers increase by 0.4%, a decrease of up to 22% was observed. This also indicates an adherence deficiency from the fiber volume and a weak union strength of plastic fibers and cement.
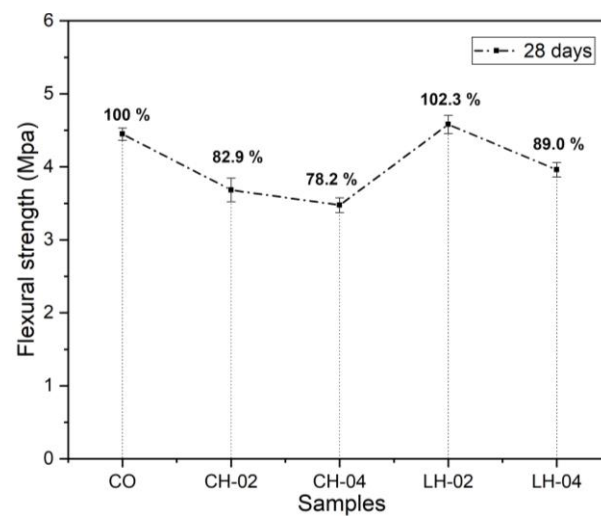
Figure 9. Effect of HDPE fibers on flexural strength.

The HDPE fiber-reinforced concrete structure after rupture is presented in Figure 10, showing the fiber distribution occurring randomly during concrete manufacturing. The red circles show the fibers' fragile union to the cement matrix detaching completely. This alters the material mechanical properties.
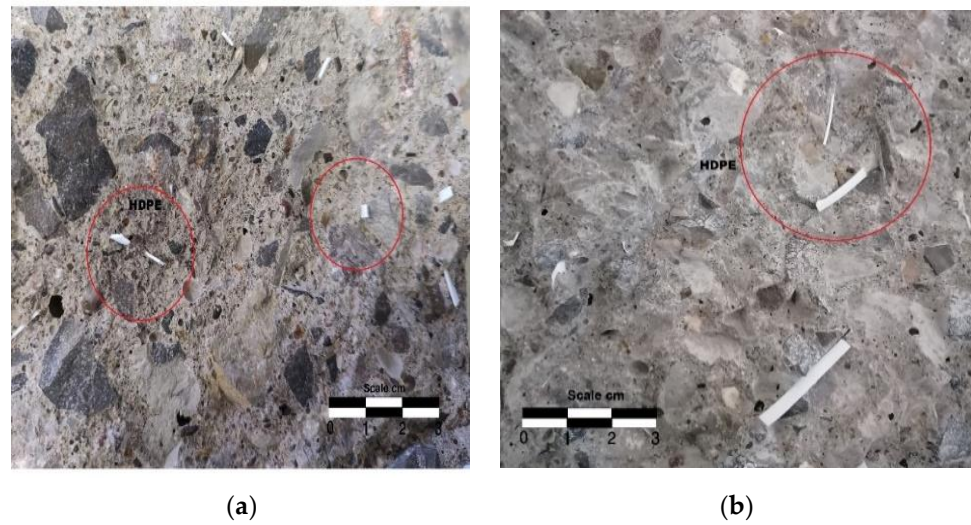
(**a**)   (**b**)

Figure 10. Concrete structure: (**a**) short fibers and (**b**) long fibers.

3.5. Half-Cell Potential Measurements

Figure 11 shows the results of corrosion potential in reinforced concrete, and with the values obtained, it is possible to diagnose the degree of corrosion of the rebars embedded in the concrete [63]. In the first 10 days of immersion, for the samples with synthetic fibers, more negative Ecorr values of between −300 mV and −520 mV were observed, suggesting a 90% probability of corrosion in the rod. This could be due to the porosity of the cement paste, where chloride ions diffuse through the pores and interact with the steel/concrete interface. Over time, all the samples present low and high peaks but maintain negative values; the potential decreases as the chloride ion content increases [69], except for specimen CH-02 at 120 days. As time progresses, the CO control sample has higher corrosion potentials compared with the concrete fiber samples. At the end of the 365 days of monitoring, all samples have a 90% corrosion probability, indicating a high interaction of chloride ions in the steel bar.
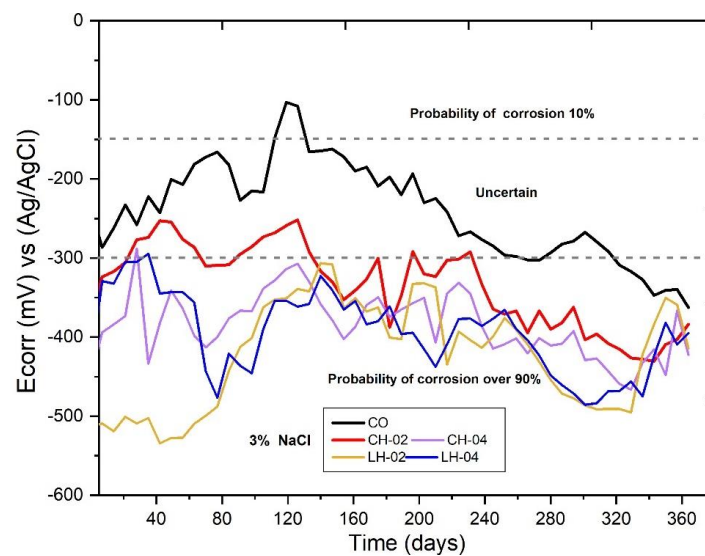

Figure 11. Average values of corrosion potentials (Ecorr).

3.6. Electrochemical Noise Measurements

The results of the current electrochemical noise resistance monitoring are shown in Figure 12a. For the interpretation of statistical data, the linear trend in current was removed as it is likely that this technique leaves some of the direct current drift behind [70]. High

and low fluctuations in Rn can be seen in the first days of monitoring for the fibrous mixtures with values between 1×10^5 and 1×10^{10} $\Omega \cdot cm^2$. The CO sample shows low Rn values, indicating a concentration of chloride ions (Cl^-) in the metal, breaking the passive layer and increasing the corrosion rate of the steel. Over time, increasing and decreasing trends are observed in all the samples, which could indicate that the bars have passivation and depassivation due to the high Cl^- content. At the end of 365 days of measurement, the samples with short fibers in smaller and larger quantities show better Rn resistance compared with the control sample. This result indicates that the HDPE fibers benefit the corrosion behaviors. The calculation of the corrosion rate V_{corr} is determined from the corrosion current density (i_{corr}) and by Faraday's law according to the following Equation (11) [71]:

$$v_{corr} = k \left(\frac{p_{eq}}{\rho} \right) \times i_{corr},$$

(11)

where V_{corr} is expressed in (mm/year), k has a value of 3.225×10^{-3} and is the conversion factor, P_{eq} is the equivalent weight of the material expressed in (g/eq), ρ is the density of the material expressed in (g/cm^2), and i_{corr} is the corrosion current density in $\mu A/cm^2$. Replacing the values for the steel corrosion study, the equation is as follows (Equation (12)):

$$v_{corr} = 0.0116 \times i_{corr}$$

(12)

Figure 12b shows the values of the corrosion rate (mm/year), which are inversely proportional to *Rn*, i.e., for higher values of EN, the corrosion rate decreases, and the entry of Cl^- into the concrete increases the rate by reducing the alkaline hydrated cement products that passivate (i.e., protect) the embedded steel [72].

Another statistical parameter is the type of corrosion shown in Figure 13, where it can be noticed that all the samples present values close to 0.9 and 1, indicating a localized type of corrosion on the metal surface and pitting initiation due to the concentration of free chlorides concentrating in specific points on the metal surface. This type of corrosion is more likely to occur in reinforced concrete structures exposed to saline environments [73].
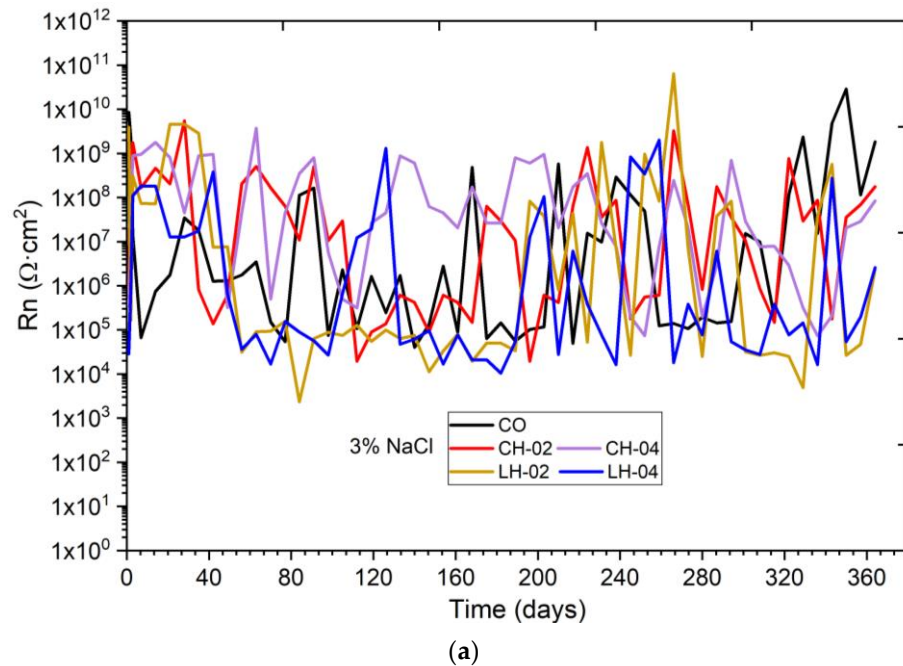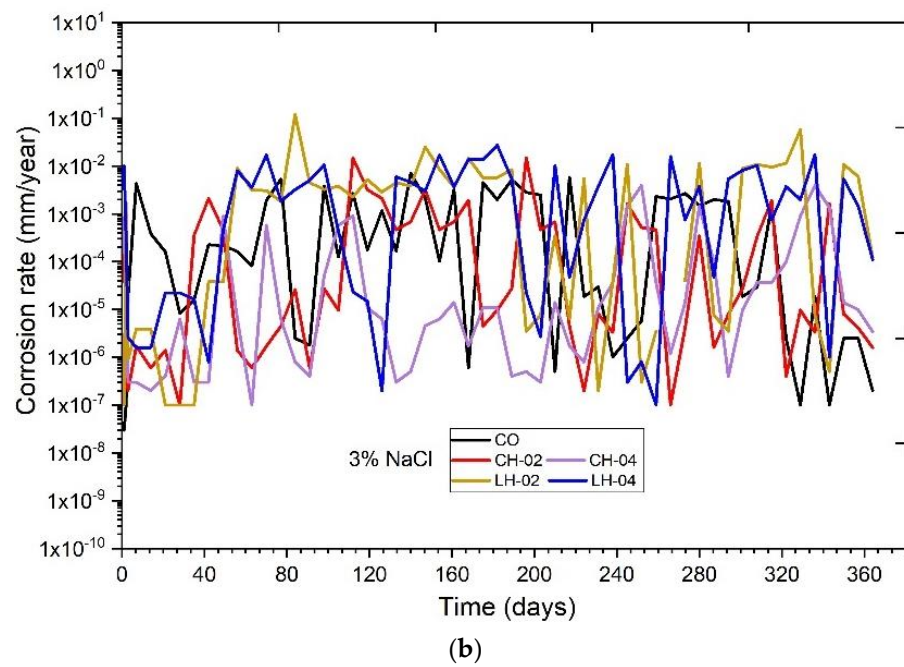

(a)

Figure 12. *Cont.*

(**b**)

Figure 12. EN values: (**a**) noise resistance and (**b**) corrosion rate.
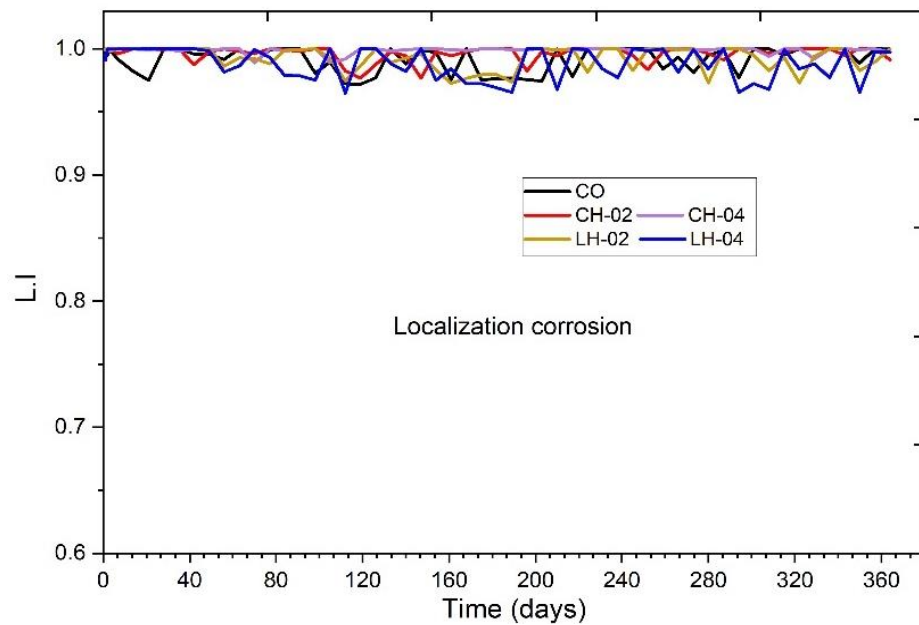

Figure 13. Location index (L.I) values on the surface of the reinforced steel.

3.7. Linear Polarization Resistance Measurements

The dimension and quantity of HDPE fibers' effects on the LPR are shown in Figure 14. It can be noticed that the long fibers have a low Rp trend during the first days, with values of 1×10^3 and 1×10^4 $\Omega \cdot cm^2$ indicating a higher corrosion rate in the metal due to high porosity and, consequently, a greater presence of oxygen diffusion in the steel/paste interaction, feeding the cathodic reaction of the metal [74]. The short fibers at the beginning of the monitoring have a high Rp trend of 1×10^4 and 1×10^5 $\Omega \cdot cm^2$, where it can be said that the steel is in a passive corrosion state. On days 160 and 360 of exposure, sample CH-02 remains at constant values of 1×10^4 $\Omega \cdot cm^2$; this trend could mean that the corrosion rate

is slow. High and low Rp values in a short time indicate a breakdown of the passive layer and a re-passivation or formation of less protective oxide layers.
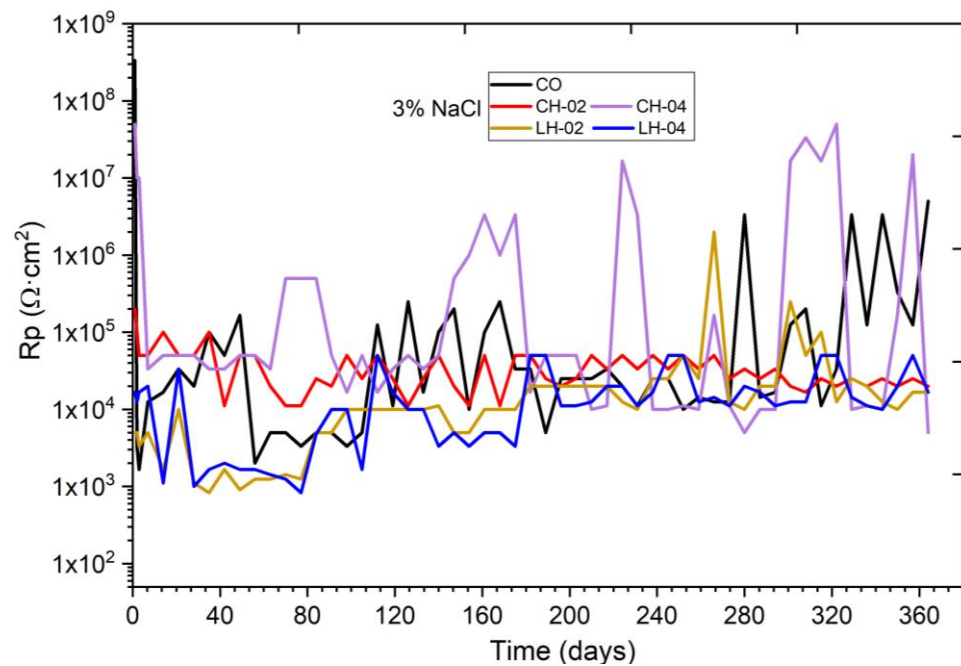
Figure 14. Graph of polarization resistance (Rp) in reinforced concrete.

The corrosion propagation phase in concrete steel in chloride conditions was estimated with the current density (i_{corr}) from the Rp values, and the results are presented in Figure 15. It can be noticed that the samples with long fibers present high values of i_{corr} between 1 and 10 $\mu A/cm^2$, suggesting severe corrosion in the metal; similar results have been found by other authors [75]. This fact may seem to be a considerable loss of the reinforcement section; however, the "localized" corrosion mechanism in the L.I results leads to a maximum activity at the edges of the anodic area, and as a result, the anodic area extends in length instead of in depth [76]. As time progresses, the samples with long fibers decrease their i_{corr} values to less than 1 $\mu A/cm^2$ and 0.5 $\mu A/cm^2$, suggesting a high to negligible corrosion. Samples CH-02 and CH-04 present current density values of 1 and 0.01 $\mu A/cm^2$ from the beginning to the end of the monitoring. This could be attributed to different factors such as the fiber dimension being randomly distributed, delaying the diffusion of chloride ions, and also the lower permeability, which generates lower porosity and avoids the concentration and interaction between oxygen and the steel bar.
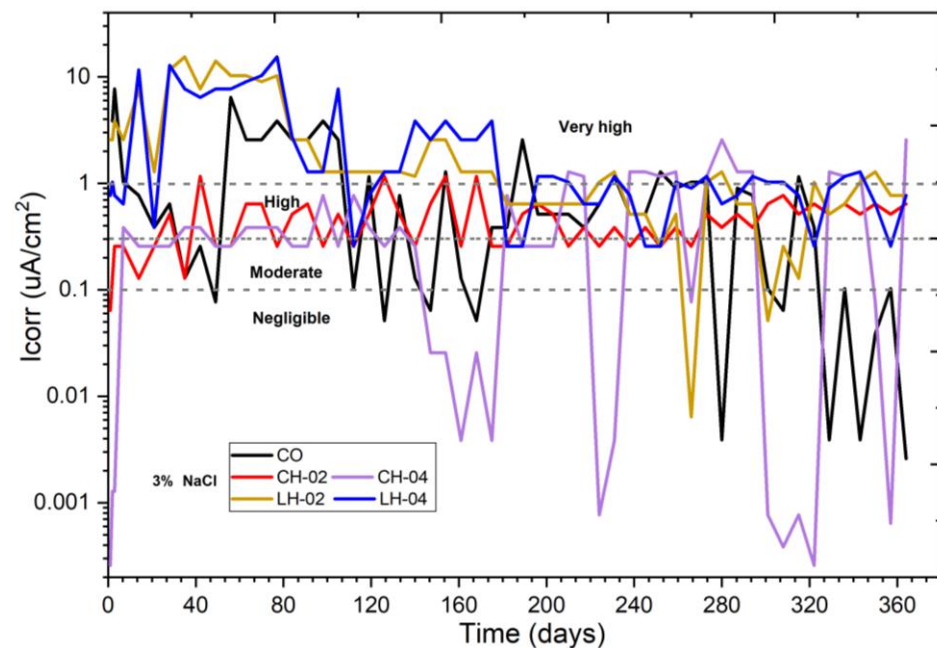
Figure 15. Estimation of the service life of the reinforced concrete.

3.8. Electrochemical Impedance Spectroscopy Measurements

This EIS technique is accurate, reproducible, and suitable for highly resistive elements such as concrete [64]. The results are represented through Nyquist plots or impedance spectra, where Zreal (Z') is observed on the abscissa and Zimaginary (Z") on the ordinate, measured at various frequencies (usually between 100 kHz and 10 mHz) [77], and the Bode plot presents the total impedance in the ordinate against the frequency in the abscissa. To interpret the EIS data, one starts from the origin point of the graph where the data measured at high frequency are presented and generate loops or capacitive semicircles, which is attributed to the bulk concrete resistance representing the ohmic resistance of the solution in the pores or cracks of the cement matrix [78]. The curve shifts to the right, which is governed by medium and low frequencies that reflect the changes that are generated at the steel/concrete interface as charge transfer is exhibited.

In Figure 16, the impedance spectra are shown, where it can be noticed that at the beginning of the scanning measurement, the CO sample presents a first semicircle and a second depressed semicircle at medium and low frequencies. If this is significantly reduced, then there is a corrosion process of the steel [64]. A higher impedance can be noticed in comparison with the mixtures with fibers; similarly, the displacement of the origin or resistance solution (Rs) of the pores is very high indicating, that the steel is passivated. However, as the exposure time advances to, for example, 365 days of immersion, a decrease in the Rs can be observed in addition to a decrease in impedance. This fact may indicate the diffusion by oxygen and free chloride ions within the concrete matrix because the straight line on the graph at low frequencies indicates a mechanism of diffusion by oxygen [79].

For the samples CH-02, LH-02, and LH-04, it is observed, at the beginning (day 1, Figure 16a), that the radii of the capacitive arcs are small. The radius of the semicircular arc is associated with the polarization resistance (*Rp*) of the passive film [80], indicating an active corrosion in the reinforcing steel. However (day 28), sample CH-04 presents a larger capacitive arc radius in addition to a larger displacement of the origin, indicating a high *Rs* and *Rp*; this may be related to the dimension of the HDPE fibers, causing a wall or barrier effect in the transport of chloride ions. At 168 and 245 days, passivation is observed for samples CH-04 (day 168, Figure 16c) and LH-04 (day 245, Figure 16d) based on the high impedance value observed.
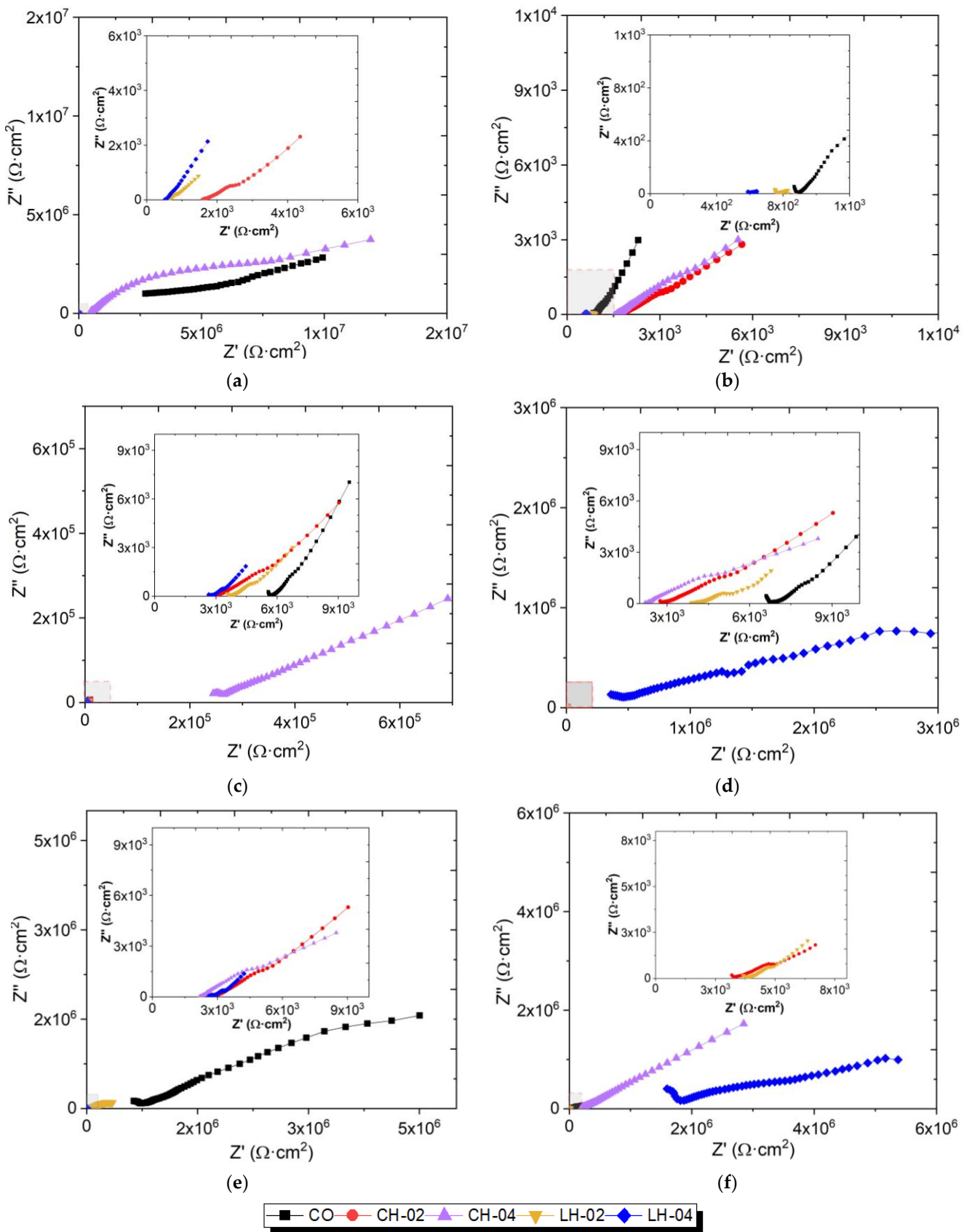
Figure 16. Nyquist diagrams for days (**a**) 1, (**b**) 28, (**c**) 168, (**d**) 245, (**e**) 280, and (**f**) 365.

Figure 17 shows the results of the Bode phase plots. At high frequencies, the impedance can be used to determine the resistance of the electrolyte or concrete solution Rs based on the electrode reaction time, and at medium and low frequencies, depolarization resistance to the steel rebar and polarization due to diffusion and movement of substances [81]. It can be observed that immersion at 24 h (Figure 17a), in the low-frequency region, high values of the impedance modulus between 1×10^6 and 1×10^7 $\Omega \cdot cm^2$ were obtained for the CO and CH-04 specimens. The high values in this low-frequency region may be associated with the presence of the passive film [82,83] and the continuous hydration of the cement. On days 245, 280, and 365 of the exposure period, the advance of the CH-04 specimens in saline medium shows that the increased and decreased *Rs* and *Rp* values between 1×10^6 and 1×10^3 indicate passivation and depassivation at the steel/concrete interface; this phenomenon could occur due to the concentration of Cl^-, as well as the LH-04 sample.
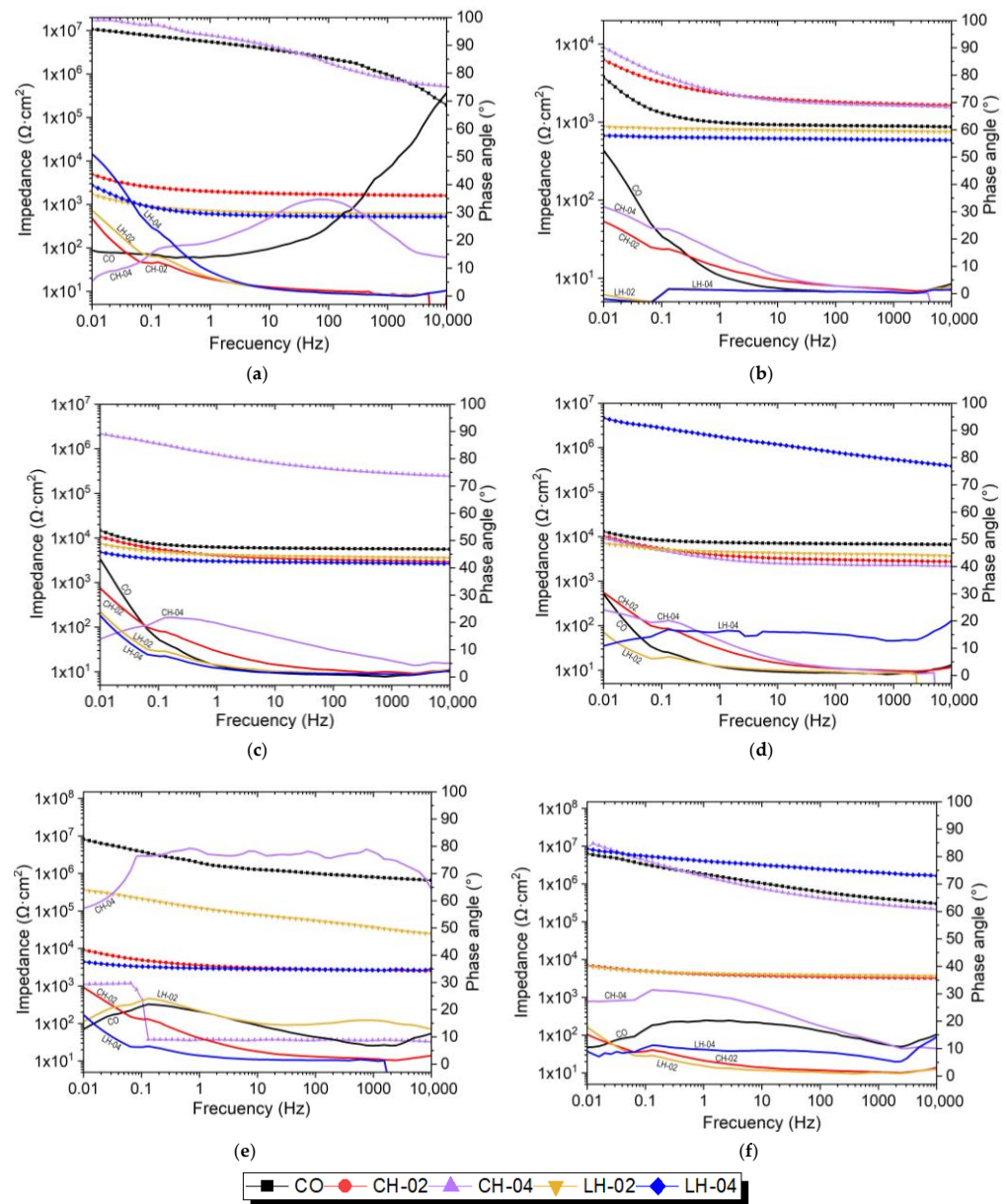

Figure 17. Electrochemical impedance and phase angle diagram of days (**a**) 1, (**b**) 28, (**c**) 168, (**d**) 245, (**e**) 280, and (**f**) 365.

4. Discussion

4.1. Effect of Slump and Porosity of Concrete with HDPE

Workability is the key parameter of the concrete mix; in a fresh state, it determines the ease and homogeneity of the concrete and also influences how it can be mixed, placed, consolidated, etc. [84]. Workability is influenced by the water content, the shape and size of the aggregates, the cement, and the types of fibers used [85]. A decrease in slump was demonstrated when the amount of HDPE plastic replacement for sand weight in concrete increased; this was consistently independent of the type of plastic added, and these effects are similar to those reported by other authors [22,29,86]. The high content and surface area of fibers can absorb more cement paste to envelop, creating greater interlock between aggregates, which in turn leads to increased viscosity and decreased slump of a concrete mix [87–89]. By adding fibers in amounts of 0.4% with respect to the weight of sand, a decrease in slump from 140 mm to 100 mm and 90 mm was observed; the decrease in slump was due to the stiffness, cohesion, and adhesion provided by the fibers in the concrete [87]. Similarly, the air content results in Table 7 showed that samples LH-04 and CH-04, with higher fiber percentages, could increase or decrease voids in the cement matrix depending specifically on a bad or good distribution of fibers in the cement paste.

Figure 6 shows that the porosity percentages are directly related to the air content in the cement matrix, i.e., the higher the air content, the higher the porosity. The increase in porosity is due to the presence of larger particles along the interior structure of the concrete and the interruption of the continuity of the microstructure of the material, resulting from the inclusion of heterogeneities in a relatively homogeneous matrix, and cavities formed in the interfacial transition zone between cement paste and plastic aggregate [84]. It is important to know these physical parameters because concrete porosity is inversely related to strength [90].

4.2. Flexural and Compressive Mechanical Properties of Concrete with HDPE Fibers

Studies have indicated a relationship between the plastic content and mechanical properties of concrete [29,89,91]. The compressive and tensile strength properties of concrete reach between 75 and 80% of its total strength during the first 28 days [92]. In this case, as shown in Figure 7, it was found that short geometries and a lower content (0.2%) of HDPE fibers increase the compressive strength of concrete by 4.8%. With the increase in fiber volume fraction, the concrete mix becomes a hard mix that has more void formation, and the mechanical bond of the cement matrix is low, leading to poor concrete strength [93,94]. As in the case of the samples with long fibers, i.e., LH-02 and LH-04, a decrease of between 9 and 12% was obtained. It was shown that the compressive strength of concrete depends on fiber length, area, and fiber volume content. These results agree with those reported by other researchers [22,95,96].

Fibers in the crack plane play a very important role in crack stability and crack growth formation [93]. They function as initiators of microcracking due to their low modulus of elasticity compared with ordinary cement [94]. Figure 8 compares the crack formation for the control sample with the HDPE fiber content. It was found that the C0 sample recorded a brittle failure, and the stresses occurred at protruding points of the application faces (top), keeping half of the cylinder intact [43,67]. Sample LH-04 presented greater crack formation throughout the cylinder patterns, which is one of the indicators of the effects of fibers in developing a crack-resistant mechanism and changing the nature of the material from brittle to ductile [97]. These findings support other studies that showed that fibers can prevent brittle failure and improve the ductility of concrete [29,98,99]. Flexural strength is an important parameter in the mechanical properties of concrete; Figure 9 describes these values and percentages. A slight increase of 2.3% was shown for long fibers with lower content. These results have similarities with other researchers who compared an analog percentage of fibers added to concrete [21,22].

The increase in flexural strength could be due to improved bonding of the aggregate to cement [100], where fibers with higher bond strength could be used in structural concrete

applications [22]. The findings in this study for flexural strength indicate that longer fibers delay cracking because the crack path changes as the plastic fiber is encountered as a barrier. In addition, there is no direct proportional relationship between the flexural and compressive mechanical properties because the fiber size largely determines the results due to the position of the plastic particles [29].

4.3. Corrosion of Reinforcing Steel in Concrete with HDPE Fibers

The corrosion rate of reinforcing steel is measured through different electrochemical parameters. One of them is the corrosion potential, also called half-cell potential (HCP), which is a non-destructive technique where the positive pole of the high-impedance voltmeter is electrically connected to the reinforcing steel and the other pole is attached to a reference electrode [72]. Figure 11 shows all the samples of concrete with HDPE fibers, which were monitored for 365 days. The corrosion occurs in terms of the following two phases: the corrosion initiation phase and the corrosion propagation phase. The first term refers to the amount of time it takes for external aggressors to initiate their attack action and the second is the destruction of the metal [101]. It was shown that the long HDPE fibers presented a trend with more negative values compared with the control sample and also had a higher probability of initiating the first phase; this fact could be due to the diffusion of chloride ions through the pores of the cement matrix. These results are similar to those reported by other authors [102,103].

Electrochemical noise measurements provide information on the mechanism and rate of corrosion in identified areas of concrete structures [104]. The signals can be examined through various mathematical methods, including spectral analysis and statistical analysis [105]. Figure 12a shows the noise measurements related to the incorporation of HDPE fibers into the cement paste, where high and low signals of electrochemical noise resistance are presented. These values range from a minimum to a maximum of 1×10^5 and 1×10^{10} $\Omega \cdot cm^2$, where high values of Rn indicate passivation in the metal and a negligible corrosion rate, which may be due to the formation of oxide films on the surface of the rebar [63]. These values are related to the corrosion rate, as shown in Figure 12b. The corrosion rate is inversely proportional to the R_n values obtained.

The drop in Rn could indicate that the concentration of chloride ions increases on the surface of the steel bar; consequently, the corrosion rate is severe [106]. In Figure 13, the type of corrosion is evident for all samples. Localized corrosion in rebar leads to different behaviors because corrosion conditions are not uniformly distributed along the element. When localized corrosion occurs, the macro cell current flows between the corroded areas (anode) of the rebar configuration and the non-corroded areas (cathode) [104,107].

Figure 14 shows the LPR measurements, demonstrating that samples with long fibers acquire low *Rp* values of 1×10^3 $\Omega \cdot cm^2$ in the first days of immersion. Physical properties such as porosity, air content, or permeability directly affect the corrosion rate. Because of the increase in these phenomena, there are larger voids in the cement matrix causing not only the increase in Cl^- diffusion but also O_2 and H_2O diffusion channels [60]. Samples with short fibers in the early stages of monitoring tend to have slightly higher values of 1×10^4 $\Omega \cdot cm^2$ compared with long fibers, indicating that the corrosion process is slow. As the exposure time progressed on day 365, an increase in the *Rp* values was observed for the long fibers between 1×10^4 and 1×10^5 $\Omega \cdot cm^2$, while the short fibers kept their values constant; this finding is important because it indicates that the plastic fibers positively affect the corrosion rate of the reinforcement. Possibly, they act as a physical barrier preventing the chloride ions found inside the paste, because of the porosity, from advancing towards the surface of the metal, and the rate is much lower. Thus, the dimension and the amount of fibers have a direct influence on the degree of corrosion of the reinforcing bars in concrete [102].

Another electrochemical method for estimating corrosion phenomena in reinforced concrete is the EIS technique. The Nyquist diagrams show capacitive arcs and typical frequencies of each corrosion phenomenon. The low frequencies allow for attributing the

low-frequency loop to a charge transfer process in combination with a mass transport process [108]; the medium frequencies correspond to the concrete strength and are related to the characteristics of the concrete environment and reinforcement protection; and the high frequencies are associated with the electrolyte resistance (*Rs*) [64]. It was shown that samples LH-02 and LH-04 presented low impedance values in the first days of monitoring and small capacitive arcs at high and medium frequencies. Compared with the control sample, the *Rs* decreased, which could be attributed to a higher infiltration of salts and an increase in the mass transport rate of dissolved oxygen within the concrete [109,110]. It was observed that these parameters increased with increasing exposure time; this phenomenon could be attributed to the precipitation of corrosion products within the pores that exist at the concrete–steel interface [110]. For the samples with short fibers, CH-02 presented, at the beginning of the exposure, capacitive arcs of the impedance of larger diameter, as well as high values of Rs, indicating a lower corrosion rate in the reinforcing rod compared with the samples with long fibers. During the 245 days, a drop in these parameters was observed, and finally, at day 365 an increase was observed. The sequence of these values over the course of time may indicate the passivation and depassivation of the steel.

HDPE fibers added to concrete have positive effects on corrosion phenomena when exposed to saline environments by delaying the transport of chloride ions, which are one of the main factors in the deterioration of the durability of concrete structures. They also improve the mechanical properties of concrete, specifically avoiding the formation of cracks and reducing the corrosion rate because they decrease the diffusion of O_2 and H_2O at the steel/concrete interface.

5. Conclusions

The following conclusions are described:

- The mechanical properties of the recycled fibers showed a decrease in tensile strength and toughness.
- Cement paste workability diminished with the increase in HDPE fibers of 20 and 35%, with respect to the control sample, from length and the interaction between fibers with aggregates.
- The air content or voids in the mix decreased for fibers with short geometry and less volume due to the fine distribution of polymer particles within the concrete structure. Concrete porosity is directly related to the number of voids; that is, porosity diminishes when fiber volume and particle length are lower.
- For concrete compressive strength, short-length fibers and a 0.2% content with respect to sand are recommended. This is because the sample presents a better mechanical response of 4.8% f'c compared with the control sample, thus retarding the cracking produced from applied stresses during the test.
- A slight 2.3% increase in concrete flexural strength for long fibers and low stress was observed, thus retarding the concrete cracking without a direct relationship to compression properties.
- A fragile adherence in the fiber/cement interface of concrete paste was evidenced by the complete detachment from the cement matrix. The fibers did not present damage or degradation from mechanical tests, and the concrete had high alkalinity and, therefore, longer durability.
- In the HCP technique, all samples showed a 90% probability of corrosion due to increased corrosion potentials.
- Samples with short HDPE fiber dimensions showed high and low Rn values between 1×10^5 and 1×10^{10} $\Omega \cdot cm^2$ during the 365 days of exposure, indicating that the steel bars were passivated and depassivated by the interaction between Cl^- and localized corrosion.
- The short fiber dimension and quantity had a direct influence on the degree of corrosion of the reinforcing bars in the concrete, presenting high Rp values and suggesting a concrete lifetime between high and negligible.

- The short fiber dimension and quantity had a direct influence on the degree of corrosion of the reinforcing bars in the concrete, presenting high Rp values and suggesting a high concrete lifetime.
- In the low-frequency EIS technique, all samples were observed to be diffusion-controlled due to Cl⁻ at the steel/concrete interface.

6. Recommendations

For possible future research, the authors recommend studies with different percentages of fibers higher than 1% by weight of the stone aggregates. In addition to the results of this research, it is important to analyze different fiber geometries and their areas, i.e., rectangular or square fibers, for use in concrete structures. The authors recommend that the length, thickness, and width of the fibers be described in detail.

There are no limitations to the specific use of synthetic waste. There are other types of plastics such as PET, LDPE, PP, and PVC that are an exponential pollutant worldwide. These plastics can be incorporated into concrete mixes and may result in the same sustainable and environmentally friendly material.

For concrete durability purposes, studies can be carried out in different aggressive atmosphere media.

References

1. Tittarelli, F.; Moriconi, G. The effect of silane-based hydrophobic admixture on corrosion of reinforcing steel in concrete. *Cem. Concr. Res.* **2008**, *38*, 1354–1357. [CrossRef]
2. Mi, T.; Wang, J.J.; McCague, C.; Bai, Y. Application of Raman Spectroscopy in the study of the corrosion of steel reinforcement in concrete: A critical review. *Cem. Concr. Compos.* **2023**, *143*, 105231. [CrossRef]
3. Gartner, N.; Kosec, T.; Legat, A. Monitoring the corrosion of steel in concrete exposed to a marine environment. *Materials* **2020**, *13*, 407. [CrossRef] [PubMed]
4. Cai, R.; Han, T.; Liao, W.; Huang, J.; Li, D.; Kumar, A.; Ma, H. Prediction of surface chloride concentration of marine concrete using ensemble machine learning. *Cem. Concr. Res.* **2020**, *136*, 106164. [CrossRef]
5. Obot, I.B.; Onyeachu, I.B.; Zeino, A.; Umoren, S.A. Electrochemical noise (EN) technique: Review of recent practical applications to corrosion electrochemistry research. *J. Adhes. Sci. Technol.* **2019**, *33*, 1453–1496. [CrossRef]
6. Li, P.; Wang, X.; Su, M.; Zou, X.; Duan, L.; Zhang, H. Characteristics of plastic pollution in the environment: A review. *Bull. Environ. Contam. Toxicol.* **2021**, *107*, 577–584. [CrossRef] [PubMed]
7. Frías, A.C.; Lema, I.I.; García, A.G. La situación de los envases de plástico en México. *Gac. Ecol.* **2003**, *69*, 67–82.
8. Bond, T.; Ferrandiz-Mas, V.; Felipe-Sotelo, M.; Van Sebille, E. The occurrence and degradation of aquatic plastic litter based on polymer physicochemical properties: A review. *Crit. Rev. Environ. Sci. Technol.* **2018**, *48*, 685–722. [CrossRef]
9. Soleimani, Z.; Gharavi, S.; Soudi, M.; Moosavi-Nejad, Z. A survey of intact low-density polyethylene film biodegradation by terrestrial Actinobacterial species. *Int. Microbiol.* **2021**, *24*, 65–73. [CrossRef]
10. Harper, C.A.; Petrie, E.M. *Plastics Materials and Processes: A Concise Encyclopedia*; John Wiley & Sons: Hoboken, NJ, USA, 2003.
11. Karaagac, E.; Koch, T.; Archodoulaki, V.M. The effect of PP contamination in recycled high-density polyethylene (rPE-HD) from post-consumer bottle waste and their compatibilization with olefin block copolymer (OBC). *Waste Manag.* **2021**, *119*, 285–294. [CrossRef]

12. Rahim, N.L.; Sallehuddin, S.; Ibrahim, N.M.; Che Amat, R.; Ab Jalil, M.F. Use of plastic waste (high density polyethylene) in concrete mixture as aggregate replacement. In *Advanced Materials Research*; Trans Tech Publications Ltd.: Wollerau, Switzerland, 2013; Volume 701, pp. 265–269. [CrossRef]
13. Zhao, X.; You, F. Waste high-density polyethylene recycling process systems for mitigating plastic pollution through a sustainable design and synthesis paradigm. *AIChE J.* **2021**, *67*, e17127. [CrossRef]
14. Hınıslıoğlu, S.; Ağar, E. Use of waste high density polyethylene as bitumen modifier in asphalt concrete mix. *Mater. Lett.* **2004**, *58*, 267–271. [CrossRef]
15. Osorio Saraz, J.A.; Varón Aristizabal, F.; Herrera Mejía, J.A. Comportamiento mecánico del concreto reforzado con fibras de bagazo de caña de azúcar. *Dyna* **2007**, *74*, 69–79.
16. Kosmatka, S.H.; Panarese, W.C.; Bringas, M.S. *Diseño y Control de Mezclas de Concreto*; Instituto Mexicano del Cemento y del Concreto: Mexico City, Mexico, 1992; ISBN 0-89312-233-5.
17. Ede, A.N.; Agbede, J.O. Use of coconut husk fiber for improved compressive and flexural strength of con-crete. *Int. J. Sci. Eng. Res.* **2015**, *6*, 968–974.
18. Almeshal, I.; Tayeh, B.A.; Alyousef, R.; Alabduljabbar, H.; Mohamed, A.M. Eco-friendly concrete containing recycled plastic as partial replacement for sand. *J. Mater. Res. Technol.* **2020**, *9*, 4631–4643. [CrossRef]
19. Nibudey, R.N.; Nagarnaik, P.B.; Parbat, D.K.; Pande, A.M. Strength and fracture properties of post consumed waste plastic fiber reinforced concrete. *Int. J. Civ. Struct. Environ. Infrastruct. Eng. Res. Dev.* **2013**, *3*, 9–16.
20. Prahallada, M.C.; Prakash, K.B. Strength and workability characteristics of waste plastic fibre reinforced concrete produced from recycled aggregates. *Int. J. Eng. Res.* **2011**, *1*, 1791–1802.
21. Malagavelli, V.; Patura, N.R. Strength characteristics of concrete using solid waste an experimental investigation. *Int. J. Earth Sci. Eng.* **2011**, *4*, 937–940.
22. Pešić, N.; Živanović, S.; Garcia, R.; Papastergiou, P. Mechanical properties of concrete reinforced with recycled HDPE plastic fibres. *Constr. Build. Mater.* **2016**, *115*, 362–370. [CrossRef]
23. Hossain, K.M.A.; Hossain, M.A.; Manzur, T. Structural performance of fiber reinforced lightweight self-compacting concrete beams subjected to accelerated corrosion. *J. Build. Eng.* **2020**, *30*, 101291. [CrossRef]
24. Vidaud, I.; Frómeta, Z.; Vidaud, E. Una aproximación a los concretos reforzados con fibras. *Constr. Tecnol. Concreto* **2015**, *30*, 31.
25. Abeysinghe, S.; Gunasekara, C.; Bandara, C.; Nguyen, K.; Dissanayake, R.; Mendis, P. Engineering Performance of Concrete Incorporated with Recycled High-Density Polyethylene (HDPE)—A Systematic Review. *Polymers* **2021**, *13*, 1885. [CrossRef]
26. *ASTM C150/C150M-20*; Standard Specification for Portland Cement. ASTM International: West Conshohocken, PA, USA, 2020. [CrossRef]
27. *ASTM C136/C136M-19*; Standard Test Method for Sieve Analysis of Fine and Coarse Aggregates. ASTM International: West Conshohocken, PA, USA, 2020. [CrossRef]
28. Patel, K.; Chikkali, S.H.; Sivaram, S. Ultrahigh molecular weight polyethylene: Catalysis, structure, properties, processing and applications. *Prog. Polym. Sci.* **2020**, *109*, 101290. [CrossRef]
29. Tamrin; Nurdiana, J. The effect of recycled HDPE plastic additions on concrete performance. *Recycling* **2021**, *6*, 18. [CrossRef]
30. *ASTM D570-22*; Standard Test Method for Water Absorption of Plastics. ASTM International: West Conshohocken, PA, USA, 2022. [CrossRef]
31. Sathishkumar, T.P.; Navaneethakrishnan, P.; Shankar, S.; Rajasekar, R.; Rajini, N. Characterization of natural fiber and composites–A review. *J. Reinf. Plast. Compos.* **2013**, *32*, 1457–1476. [CrossRef]
32. *ASTM D792-20*; Standard Test Methods for Density and Specific Gravity (Relative Density) of Plastics by Displacement. ASTM International: West Conshohocken, PA, USA, 2020.
33. Awad, A.H.; El Gamasy, R.; Abd El Wahab, A.; Abdellatif, M.H. Mechanical and Physical Properties of PP and HDPE. *Eng. Sci* **2019**, *4*, 34–42. [CrossRef]
34. Barahona, C.C.; Mera, J.; Martínez, D.; Rodríguez, J. Aprovechamiento de polipropileno y polietileno de alta densidad reciclados, reforzados con fibra vegetal, Tetera (Stromanthe Stromathoides). *Rev. Polim.* **2010**, *11*, 417–427.
35. *ASTM D638-22*; Standard Test Method for Tensile Properties of Plastics. ASTM International: West Conshohocken, PA, USA, 2022. [CrossRef]
36. Dhakal, H.N.; Zhang, Z.A.; Richardson, M.O. Effect of water absorption on the mechanical properties of hemp fibre reinforced unsaturated polyester composites. *Compos. Sci. Technol.* **2007**, *67*, 1674–1683. [CrossRef]
37. Arrakhiz, F.Z.; El Achaby, M.; Kakou, A.C.; Vaudreuil, S.; Benmoussa, K.; Bouhfid, R.; Qaiss, A. Mechanical properties of high density polyethylene reinforced with chemically modified coir fibers: Impact of chemical treatments. *Mater. Des.* **2012**, *37*, 379–383. [CrossRef]
38. Foulk, J.A.; Chao, W.Y.; Akin, D.E.; Dodd, R.B.; Layton, P.A. Enzyme-retted flax fiber and recycled polyethylene composites. *J. Polym. Environ.* **2004**, *12*, 165–171. [CrossRef]
39. Colom, X.; Carrasco, F.; Pages, P.; Canavate, J. Effects of different treatments on the interface of HDPE/lignocellulosic fiber composites. *Compos. Sci. Technol.* **2003**, *63*, 161–169. [CrossRef]
40. *ASTM C143/C143M-20*; Standard Test Method for Slump of Hydraulic-Cement Concrete. ASTM International: West Conshohocken, PA, USA, 2020. [CrossRef]

41. *ASTM C231/C231M-22*; Standard Test Method for Air Content of Freshly Mixed Concrete by the Pressure Method. ASTM International: West Conshohocken, PA, USA, 2022. [CrossRef]
42. *ASTM C31/C31M19a*; Standard Practice for Making and Curing Concrete Test Specimens in the Field. ASTM International: West Conshohocken, PA, USA, 2019. [CrossRef]
43. *ASTM C39/C39M-23*; Standard Test Method for Compressive Strength of Cylindrical Concrete Specimens. ASTM International: West Conshohocken, PA, USA, 2023. [CrossRef]
44. *ASTM C78/C78M-22*; Standard Test Method for Flexural Strength of Concrete (Using Simple Beam with Third-Point Loading). ASTM International: West Conshohocken, PA, USA, 2022. [CrossRef]
45. *ASTM C876-09*; Standard Test Method for Corrosion Potentials of Uncoated Reinforcing Steel in Concrete. ASTM International: West Conshohocken, PA, USA, 2016. [CrossRef]
46. Pfändler, P.; Keßler, S.; Huber, M.; Angst, U. Spatial variability of half-cell potential data from a reinforced concrete structure—A geostatistical analysis. *Struct. Infrastruct. Eng.* **2022**, 1–16. [CrossRef]
47. Dineshkumar, R.; Harikaran, C.; Veerapandi, P. Corrosion Assessment in Reinforced Concrete Elements using Half-Cell Potentiometer—A Review. *Measurement* **2020**, *9*, 12.
48. Adriman, R.; Ibrahim, I.B.M.; Huzni, S.; Fonna, S.; Ariffin, A.K. Improving half-cell potential survey through computational inverse analysis for quantitative corrosion profiling. *Case Stud. Constr. Mater.* **2022**, *16*, e00854. [CrossRef]
49. Jamali, S.S.; Mills, D.J. A critical review of electrochemical noise measurement as a tool for evaluation of organic coatings. *Prog. Org. Coat.* **2016**, *95*, 26–37. [CrossRef]
50. Tamayo, J.M.; Chavarín, J.U. *La Técnica de Ruido Electroquímico para el estudio de la Corrosión*; Instituto de Investigaciones Eléctricas: Cuernavaca, Mexico, 2002.
51. Cottis, R.A. Interpretation of electrochemical noise data. *Corrosion* **2001**, *57*, 265–285. [CrossRef]
52. Sánchez, A.; Sanjurjo, M.; Bouzada, F.; Urrejola, S. Análisis estadístico de los registros de ruido electroquímico obtenidos en la corrosión del aluminio. *Rev. Metal.* **2005**, *41*, 330–339. [CrossRef]
53. Arellano-Pérez, J.H.; Escobar-Jiménez, R.F.; Ramos-Negrón, O.J.; Lucio-García, M.A.; Gómez-Aguilar, J.F.; Uruchurtu-Chavarín, J. The Use of a Time-Frequency Transform for the Analysis of Electrochemical Noise for Corrosion Estimation. *Math. Probl. Eng.* **2022**, *2022*, 4333607. [CrossRef]
54. Sanchez-Amaya, J.M.; Osuna, R.M.; Bethencourt, M.; Botana, F.J. Monitoring the degradation of a high solids epoxy coating by means of EIS and EN. *Prog. Org. Coat.* **2007**, *60*, 248–254. [CrossRef]
55. Stern, M.; Geary, A.L. Electrochemical polarization: I. *A theoretical analysis of the shape of polarization curves. J. Electrochem. Soc.* **1957**, *104*, 56. [CrossRef]
56. Estupiñán-López, F.H.; Almeraya-Calderón, F.; Bautista Margulis, G.R.; Baltazar Zamora, M.A.; Martínez-Villafañe, A.; Uruchurtu, C.J.; Gaona-Tiburcio, C. Transient analysis of electrochemical noise for 316 and duplex 2205 stainless steels under pitting corrosion. *Int. J. Electrochem. Sci.* **2011**, *6*, 1785–1796. [CrossRef]
57. Faritov, A.T.; Rozhdestvenskii, Y.G.; Yamshchikova, S.A.; Minnikhanova, E.R.; Tyusenkov, A.S. Improvement of the linear polarization resistance method for testing steel corrosion inhibitors. *Russ. Metall. (Met.)* **2016**, *2016*, 1035–1041. [CrossRef]
58. *ASTM G59-97*; Standard Test Method for Conducting Potentiodynamic Polarization Resistance Measurements. ASTM International: West Conshohocken, PA, USA, 2020. [CrossRef]
59. Brown, D.W.; Connolly, R.J.; Darr, D.R.; Laskowski, B. Linear Polarization Resistance Sensor Using the Structure as a Working Electrode. In Proceedings of the PHM Society European Conference, Nantes, France, 8–10 July 2014; 2.
60. Da, B.; Yu, H.; Ma, H.; Wu, Z. Reinforcement corrosion research based on the linear polarization resistance method for coral aggregate seawater concrete in a marine environment. *Anti-Corros. Methods Mater.* **2018**, *65*, 458–470. [CrossRef]
61. Baweja, D.; Roper, H.; Sirivivatnanon, V. Improved electrochemical determinations of chloride-induced steel corrosion in concrete. *Mater. J.* **2003**, *100*, 228–238.
62. Andrade, C.; Alonso, C. Corrosion rate monitoring in the laboratory and on-site. *Constr. Build. Mater.* **1996**, *10*, 315–328. [CrossRef]
63. Flores-Nicolás, A.; Flores-Nicolás, M.; Uruchurtu-Chavarín, J. Corrosion effect on reinforced concrete with the addition of graphite powder and its evaluation on physical-electrochemical properties. *Rev. ALCONPAT* **2021**, *11*, 18–33. [CrossRef]
64. Ribeiro, D.V.; Abrantes, J.C.C. Application of electrochemical impedance spectroscopy (EIS) to monitor the corrosion of reinforced concrete: A new approach. *Constr. Build. Mater.* **2016**, *111*, 98–104. [CrossRef]
65. Sobhani, J.; Najimi, M. Electrochemical impedance behavior and transport properties of silica fume contained concrete. *Constr. Build. Mater.* **2013**, *47*, 910–918. [CrossRef]
66. Solís-Carcaño, R.Ó.M.E.L.; Moreno, E.I. Análisis de la porosidad del concreto con agregado calizo. *Rev. Fac. Ing. UCV* **2006**, *21*, 57–68.
67. Nicolás, A.F. Evaluación en la Corrosión y Protección del Acero de Refuerzo Embebidas de Concreto en Presencia de Grafito y su Instituto de Investigación en Ciencias Básicas y Aplicadas Aplicadas Efecto en las Propiedades Mecánicaselectroquímicas. 2021. Available online: http://riaa.uaem.mx/xmlui/handle/20.500.12055/1554 (accessed on 16 December 2023).
68. Al-Hadithi, A.I.; Hilal, N.N. The possibility of enhancing some properties of self-compacting concrete by adding waste plastic fibers. *J. Build. Eng.* **2016**, *8*, 20–28. [CrossRef]
69. Yodsudjai, W.; Pattarakittam, T. Factors influencing half-cell potential measurement and its relationship with corrosion level. *Measurement* **2017**, *104*, 159–168. [CrossRef]

70. Li, Z.; Homborg, A.; Gonzalez-Garcia, Y.; Kosari, A.; Visser, P.; Mol, A. Evaluation of the formation and protectiveness of a lithium-based conversion layer using electrochemical noise. *Electrochim. Acta* **2022**, *426*, 140733. [CrossRef]

71. Lock, A.U. Velocidad de corrosión de aceros nacionales AISI 1010 en ácido sulfúrico como medio agresivo. *Rev. Quim.* **1991**, *5*, 21–38.

72. Almashakbeh, Y.; Saleh, E.; Al-Akhras, N.M. Evaluation of Half-Cell Potential Measurements for Reinforced Concrete Corrosion. *Coatings* **2022**, *12*, 975. [CrossRef]

73. Darmawan, M.S. Pitting corrosion model for reinforced concrete structures in a chloride environment. *Mag. Concr. Res.* **2010**, *62*, 91–101. [CrossRef]

74. Andrade, C. Propagation of reinforcement corrosion: Principles, testing and modelling. *Mater. Struct.* **2019**, *52*, 2. [CrossRef]

75. Raczkiewicz, W. Use of polypropylene fibres to increase the resistance of reinforcement to chloride corrosion in concretes. *Sci. Eng. Compos. Mater.* **2021**, *28*, 555–567. [CrossRef]

76. François, R. A discussion on the order of magnitude of corrosion current density in reinforcements of concrete structures and its link with cross-section loss of reinforcement. *RILEM Tech. Lett.* **2021**, *6*, 158–168. [CrossRef]

77. Daniyal, M.; Akhtar, S. Corrosion assessment and control techniques for reinforced concrete structures: A review. *J. Build. Pathol. Rehabil.* **2020**, *5*, 1–20. [CrossRef]

78. Song, G. Equivalent circuit model for AC electrochemical impedance spectroscopy of concrete. *Cem. Concr. Res.* **2000**, *30*, 1723–1730. [CrossRef]

79. Herrera Hernández, H.; González Díaz, F.; Fajardo San Miguel, G.D.J.; Velázquez Altamirano, J.C.; González Morán, C.O.; Morales Hernández, J. Electrochemical impedance spectroscopy as a practical tool for monitoring the carbonation process on reinforced concrete structures. *Arab. J. Sci. Eng.* **2019**, *44*, 10087–10103. [CrossRef]

80. Zhao, W.; Zhao, J.; Zhang, S.; Yang, J. Application of Electrochemical Impedance Spectroscopy to Evaluate the Corrosion Behavior of 2304 Duplex Stainless Steel Reinforced Rebar in Concrete Exposed in Chloride-Rich Environment. *Int. J. Electrochem. Sci.* **2019**, *14*, 8039–8047. [CrossRef]

81. Park, J.; Jung, M. Evaluation of the corrosion behavior of reinforced concrete with an inhibitor by electrochemical impedance spectroscopy. *Materials* **2021**, *14*, 5508. [CrossRef] [PubMed]

82. Fattah-Alhosseini, A.; Taheri Shoja, S.; Heydari Zebardast, B.; Mohamadian Samim, P. An electrochemical impedance spectroscopic study of the passive state on AISI 304 stainless steel. *Int. J. Electrochem.* **2011**, *2011*, 152143. [CrossRef]

83. Cellat, K.; Tezcan, F.; Beyhan, B.; Kardaş, G.; Paksoy, H. A comparative study on corrosion behavior of rebar in concrete with fatty acid additive as phase change material. *Constr. Build. Mater.* **2017**, *143*, 490–500. [CrossRef]

84. Bahij, S.; Omary, S.; Feugeas, F.; Faqiri, A. Fresh and hardened properties of concrete containing different forms of plastic waste–A review. *Waste Manag.* **2020**, *113*, 157–175. [CrossRef] [PubMed]

85. Vadivel, T.S.; Doddurani, M. An experimental study on mechanical properties of waste plastic fiber reinforced concrete. *Int. J. Emerg. Trends Eng. Dev.* **2013**, *3*, 395–401.

86. Abu-Saleem, M.; Zhuge, Y.; Hassanli, R.; Ellis, M.; Rahman, M.; Levett, P. Evaluation of concrete performance with different types of recycled plastic waste for kerb application. *Constr. Build. Mater.* **2021**, *293*, 123477. [CrossRef]

87. Fallah, S.; Nematzadeh, M. Mechanical properties and durability of high-strength concrete containing macro-polymeric and polypropylene fibers with nano-silica and silica fume. *Constr. Build. Mater.* **2017**, *132*, 170–187. [CrossRef]

88. Chen, B.; Liu, J. Contribution of hybrid fibers on the properties of the high-strength lightweight concrete having good workability. *Cem. Concr. Res.* **2005**, *35*, 913–917. [CrossRef]

89. Hossain, F.Z.; Shahjalal, M.; Islam, K.; Tiznobaik, M.; Alam, M.S. Mechanical properties of recycled aggregate concrete containing crumb rubber and polypropylene fiber. *Constr. Build. Mater.* **2019**, *225*, 983–996. [CrossRef]

90. Özcan, F.; Koç, M.E. Influence of ground pumice on compressive strength and air content of both non-air and air entrained concrete in fresh and hardened state. *Constr. Build. Mater.* **2018**, *187*, 382–393. [CrossRef]

91. Kakooei, S.; Akil, H.M.; Jamshidi, M.; Rouhi, J. The effects of polypropylene fibers on the properties of reinforced concrete structures. *Constr. Build. Mater.* **2012**, *27*, 73–77. [CrossRef]

92. Yaakob, M.Y.; Kamarudin, M.H.; Salit, M.S.; Pieter, H.H.I.; Badarulzaman, N.A.; Sohaimi, R.M. A review on different forms and types of waste plastic used in concrete structure for improvement of mechanical properties. *J. Adv. Res. Appl. Mech.* **2016**, *28*, 9–30.

93. Anandan, S.; Alsubih, M. Mechanical strength characterization of plastic fiber reinforced cement concrete composites. *Appl. Sci.* **2021**, *11*, 852. [CrossRef]

94. Richardson, A.E. Compressive strength of concrete with polypropylene fibre additions. *Struct. Surv.* **2006**, *24*, 138–153. [CrossRef]

95. Sharma, R.; Bansal, P.P. Use of different forms of waste plastic in concrete—A review. *J. Clean. Prod.* **2016**, *112*, 473–482. [CrossRef]

96. Ahmad, J.; Majdi, A.; BabekerElhag, A.; Deifalla, A.F.; Soomro, M.; Isleem, H.F.; Qaidi, S. A step towards sustainable concrete with substitution of plastic waste in concrete: Overview on mechanical, durability and microstructure analysis. *Crystals* **2022**, *12*, 944. [CrossRef]

97. Bhogayata, A.C.; Arora, N.K. Fresh and strength properties of concrete reinforced with metalized plastic waste fibers. *Constr. Build. Mater.* **2017**, *146*, 455–463. [CrossRef]

98. Awad, H.K. Influence of Cooling Methods on the Behavior of Reactive Powder Concrete Exposed to Fire Flame Effect. *Fibers* **2020**, *8*, 19. [CrossRef]

99. Alqahtani, F.K.; Ghataora, G.; Khan, M.I.; Dirar, S. Novel lightweight concrete containing manufactured plastic aggregate. *Constr. Build. Mater.* **2017**, *148*, 386–397. [CrossRef]

100. Mohammed, A.M.; Hammadi, A.A. Effect of adding the plastic waste as fibers on mechanical properties of concrete. *J. Eng. Sustain. Dev.* **2018**, *22*, 86–95. [CrossRef]

101. Raupach, M. Models for the propagation phase of reinforcement corrosion–an overview. *Mater. Corros.* **2006**, *57*, 605–613. [CrossRef]

102. Kakooei, S.; Akil, H.M.; Dolati, A.; Rouhi, J. The corrosion investigation of rebar embedded in the fibers reinforced concrete. *Constr. Build. Mater.* **2012**, *35*, 564–570. [CrossRef]

103. Sappakittipakorn, M.; Banthia, N. Corrosion of rebar and role of fiber reinforced concrete. *J. Test. Eval.* **2012**, *40*, 127–136. [CrossRef]

104. Song, H.W.; Saraswathy, V. Corrosion monitoring of reinforced concrete structures-A. *Int. J. Electrochem. Sci* **2007**, *2*, 1–28. [CrossRef]

105. Fan, L.; Shi, X. Techniques of corrosion monitoring of steel rebar in reinforced concrete structures: A review. *Struct. Health Monit.* **2022**, *21*, 1879–1905. [CrossRef]

106. Zhao, B.; Li, J.H.; Hu, R.G.; Du, R.G.; Lin, C.J. Study on the corrosion behavior of reinforcing steel in cement mortar by electrochemical noise measurements. *Electrochim. Acta* **2007**, *52*, 3976–3984. [CrossRef]

107. Wang, C.Y.; Shih, C.C.; Hong, S.C.; Hwang, W.C. Rehabilitation of cracked and corroded reinforced concrete beams with fiber-reinforced plastic patches. *J. Compos. Constr.* **2004**, *8*, 219–228. [CrossRef]

108. Dhouibi, L.; Triki, E.; Raharinaivo, A. The application of electrochemical impedance spectroscopy to determine the long-term effectiveness of corrosion inhibitors for steel in concrete. *Cem. Concr. Compos.* **2002**, *24*, 35–43. [CrossRef]

109. Kim, J.K.; Kee, S.H.; Futalan, C.M.; Yee, J.J. Corrosion monitoring of reinforced steel embedded in cement mortar under wet-and-dry cycles by electrochemical impedance spectroscopy. *Sensors* **2019**, *20*, 199. [CrossRef] [PubMed]

110. Shi, W.; Dong, Z.H.; Kong, D.J.; Guo, X.P. Application of wire beam electrode technique to investigate initiation and propagation of rebar corrosion. *Cem. Concr. Res.* **2013**, *48*, 25–33. [CrossRef]